Title

Electrostatics Generated by a Supramolecular Capsule Stabilizes the Transition State for Carbon—Carbon Reductive Elimination from Gold(III) Complex

Journal

The Journal of Physical Chemistry Letters, 9(14)

ISSN

1948-7185

Authors

Welborn, Valerie Vaissier

Head-Gordon, Teresa

Publication Date

2018-07-19

DOI

10.1021/acs.jpclett.8b01710

Peer reviewed

Electrostatics Generated by a Supramolecular Capsule Stabilizes the Transition State for Carbon-Carbon Reductive Elimination from Gold(III) Complex

Valerie Vaissier Welborn[1,2,3] and Teresa Head-Gordon[1-5*]

[1]Kenneth S. Pitzer Center for Theoretical Chemistry
[2]Department of Chemistry, University of California, Berkeley
[3]Chemical Sciences Division, Lawrence Berkeley National Labs, Berkeley
[4]Department of Chemical and Biomolecular Engineering and
[5]Department of Bioengineering, University of California, Berkeley
E-mail: thg@berkeley.edu

Abstract

Tetrahedral assemblies of stoichiometry M_4L_6 have been proven to catalyze a range of chemical reactions including the carbon-carbon reductive elimination reaction from transition metals such as gold. Here, we perform quantum chemical calculations of Gold(III) transition metal complexes in vacuum, and encapsulated in $Ga_4L_6^{12-}$ or $Si_4L_6^{8-}$ assemblies within both a reaction field continuum solvent and in an aqueous molecular environment with counterions, to rationalize the rate enhancements observed experimentally for the reductive elimination reaction. We find that the $Ga_4L_6^{12-}$ assembly lowers the energy barrier of the reaction compared to $Si_4L_6^{8-}$, which is consistent with kinetic trends observed experimentally. We have determined that the primary factor for catalytic rate acceleration stems from the electrostatic environment emanating from the $Ga_4L_6^{12-}$ capsule as opposed to the water or counterions.

*thg@berkeley.edu

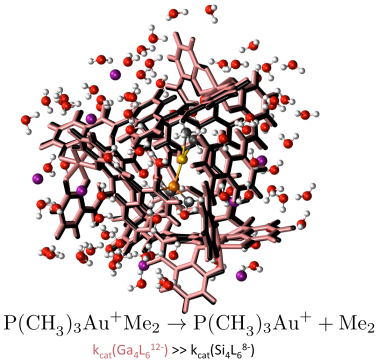

Organometallic compounds are widely used in industry to promote reactions essential to the production of man-made chemicals.[1-3] In particular, transition metal complexes are of great importance for coupling reactions that form carbon-carbon bonds.[4-6] The elementary step in these processes is the reductive elimination reaction, which reduces the oxidation state of the metal while forming the new carbon-carbon bond.[7-8] Although carbon-carbon reductive elimination from palladium, nickel, and platinum complexes is routinely exploited[9-12], the preference for a catalyzed reductive elimination reaction from gold is driven by its greater stability to air and solvent[13]. While Wolf and co-workers have established that aryl-aryl bond reductive elimination from Au(III) complexes is fast[14], the alkyl-alkyl bond reductive elimination is much slower, requires elevated temperatures, and is impeded by small amounts of free ligand[15].

Recently, Kaphan et al. established that the reductive elimination reaction using a trimethylphosphine(dimethyl)gold iodine complex, $P(CH_3)_3(CH_3)_2AuI$, could be catalyzed by a self-assembled tetrahedral complex[16], $Ga_4L_6^{12-}$ (where L=N,N'-bis(2,3-dihydroxybenzoyl)-1,5-diaminonaphtalene), previously synthesized by the Raymond group[17]. Demonstrating a Michaelis-Menten mechanism from a predissociated intermediate $P(CH_3)_3(CH_3)_2Au^+$ (Figure 1), they found that rate of reductive elimination in the presence of the $Ga_4L_6^{12-}$ complex is accelerated with $k_{cat}/k_{uncat} = 1.9 \times 10^7$. However, not much is known about the origin of the predissociation event, and the catalytic power introduced by the supramolecular capsule involving different anionic assemblies, for example $Ga_4L_6^{12-}$ vs. $Si_4L_6^{8-}$, have not been considered for the carbon-carbon reductive elimination reaction.

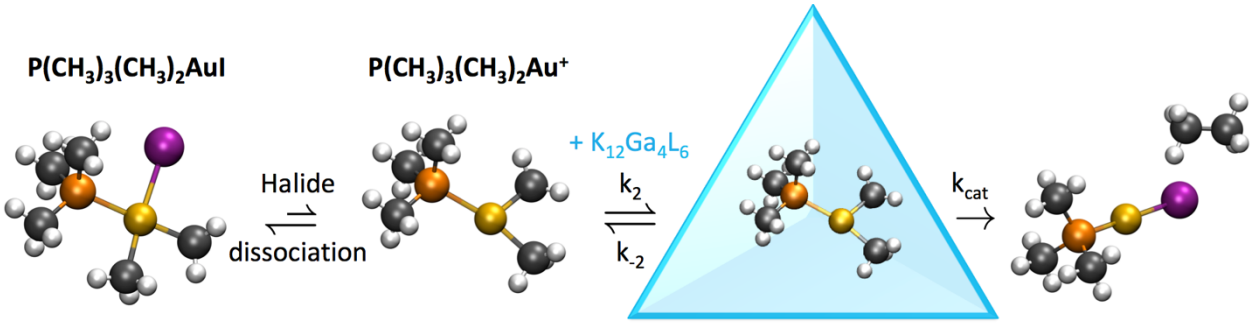

Figure 1. Proposed mechanism for the catalyzed reductive elimination of trialkylphosphine(dimethyl)gold iodine ($P(CH_3)_3(CH_3)_2AuI$) taken from ref [18]. The tetrahedral assemblies encapsulate the positively charged reaction intermediate $P(CH_3)_3(CH_3)_2Au^+$ that results from the dissociation of the iodine from the original complex.

In this work we present quantum chemical calculations of the two possible reactants, $P(CH_3)_3(CH_3)_2AuI$ and $P(CH_3)_3(CH_3)_2Au^+$, in vacuum, and compare it to when the reactants are

encapsulated within an extended environment of the tetrahedral assemblies $M_4L_6^{-n}$ where M=Si (n=8) and M=Ga (n=12), with and without explicit solvent and counterions, to gain insight into the origin of the catalytic effect on the alkyl-alkyl reductive elimination reaction.

We start by looking at the reference reaction in vacuum, that is the reductive elimination from $P(CH_3)_3(CH_3)_2AuI$ and $P(CH_3)_3(CH_3)_2Au^+$ in isolation. The reactant state (RS_i), transition state (TS_i), and product state (PS_i) structures are shown in Figure 2 for the *i* gold complex. The RS of both $P(CH_3)_3(CH_3)_2AuI$ and $P(CH_3)_3(CH_3)_2Au^+$ is planar, with one of the leaving methyl group in the trans position with respect to the phosphine ligand, while the planarity of the complex breaks in the TS for $P(CH_3)_3(CH_3)_2AuI$, but is preserved for $P(CH_3)_3(CH_3)_2Au^+$. A linear complex is then formed in the PS upon detachment of ethane, in agreement with other studies.[14]

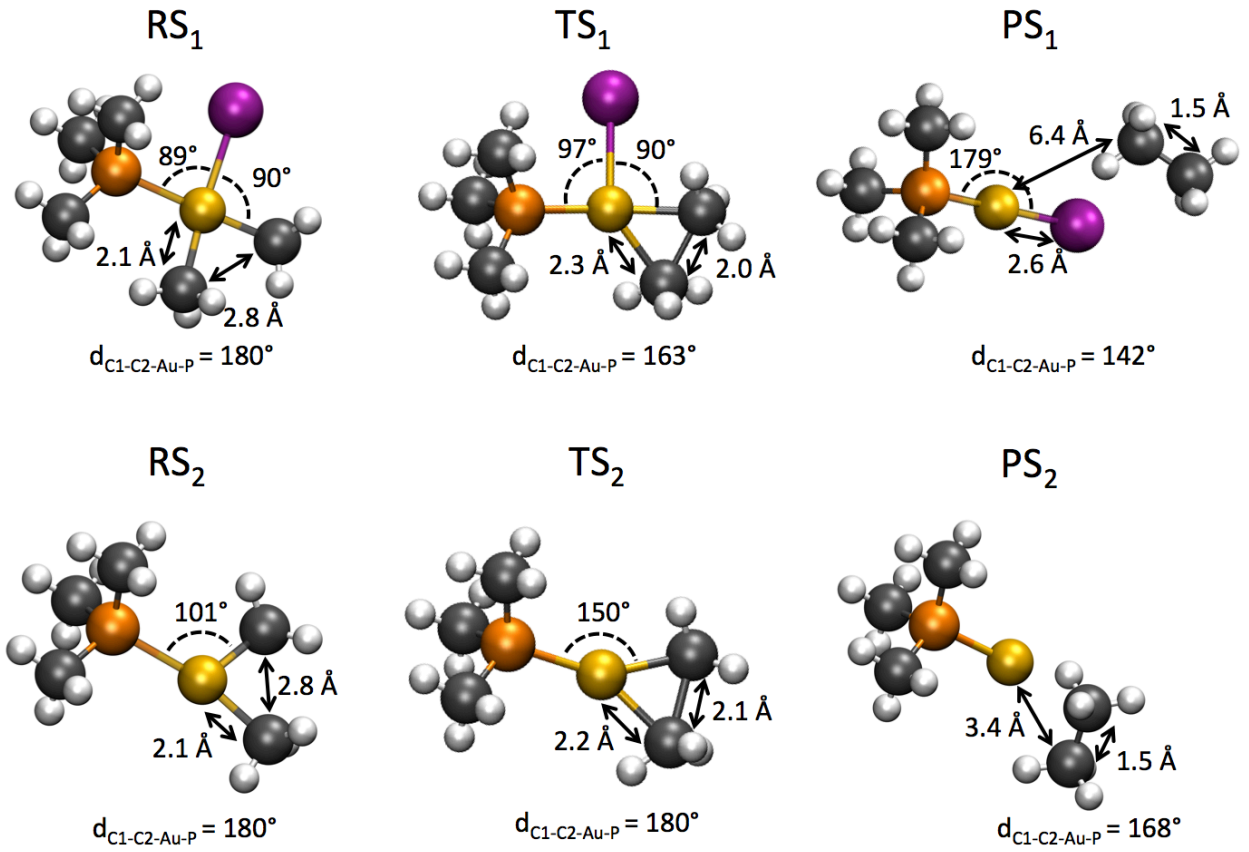

Figure 2. Geometry of the reactant, transition and product states of the direct reductive elimination reaction from $P(CH_3)_3(CH_3)_2AuI$ (RS_1, TS_1 and PS_1 - top) and $P(CH_3)_3(CH_3)_2Au^+$ (RS_2, TS_2 and PS_2 - bottom). Color key: gray=carbon, white=hydrogen, gold=gold, orange=phosphorous and purple=iodine.

In Table 1, we provide the reaction energy (ΔE) and activation energy (E_A) of these two reactants in vacuum, evaluated with a reasonably high quality GGA hybrid functional, ωB97X-v with a mixed TZV2P/DZVP basis set, for the RS, TS, and PS stationary points determined from the meta-GGA B97M-v functional using the same mixed basis. We observe that alkyl-alkyl reductive elimination is thermodynamically favorable for both complexes by close to ~25 kcal/mol. However, the reaction from $P(CH_3)_3(CH_3)_2AuI$ is hindered by a ~29-30 kcal/mol energy barrier, consistent with DFT studies for the energy barrier of 35.7 kcal/mol reported for reductive elimination from $P(CH_3)_3(CH_3)_2AuCl$.[14] Interestingly, the barrier is greatly reduced to ~1-2 kcal/mol when considering the reductive elimination from $P(CH_3)_3(CH_3)_2Au^+$.

Table 1. Reaction energy in vacuum (ΔE), solvent **(ΔE_{solv})** and activation energy (E_A) of the direct reductive elimination reaction from $P(CH_3)_3(CH_3)_2AuI$ and $P(CH_3)_3(CH_3)_2Au^+$ in vacuum and in a self-consistent reaction field model for solvent. The energies are computed with the hybrid GGA ωB97X-v level of theory with a mixed TZV2P/DZVP basis set and given in kcal/mol.

	Vacuum		**Reaction Field**	
Complex	**ΔE**	**E_A**	**ΔE_{solv}**	**E_A**
$P(CH_3)_3(CH_3)_2AuI$	-23.2	29.1	-21.5	29.8
$P(CH_3)_3(CH_3)_2Au^+$	-24.0	1.7	-6.8	0.7
	$Ga_4L_6^{12-}$ Vacuum		**$Ga_4L_6^{12-}$ Reaction Field**	
Complex	**ΔE**	**E_A**	**ΔE_{solv}**	**E_A**
$P(CH_3)_3(CH_3)_2AuI$	-40.1	32.6	-17.5	41.8
$P(CH_3)_3(CH_3)_2Au^+$	-18.3	~0	-13.8	0.6
	$Si_4L_6^{8-}$ Vacuum		**$Si_4L_6^{8-}$ Reaction Field**	
Complex	**ΔE**	**E_A**	**ΔE_{solv}**	**E_A**
$P(CH_3)_3(CH_3)_2AuI$	-40.1	22.9	-25.4	30.6
$P(CH_3)_3(CH_3)_2Au^+$	-18.3	7.6	-14.6	13.4

In either case these catalytic reactions are not possible to conduct in a vacuum, and require environmental effects that can be tuned to support and accelerate the reductive elimination reaction. Using a simple continuum model, there are clearly quantitative changes in the relative energies for the charged complex when embedded in a high dielectric medium, indicating the relevance of solvent effects, but the overall activation energy barriers remain unchanged. We therefore next consider the encapsulation of the two active site complexes $P(CH_3)_3(CH_3)_2AuI$ and $P(CH_3)_3(CH_3)_2Au^+$ in the bare $Ga_4L_6^{12-}$ and $Si_4L_6^{8-}$ (Table 1) complexes in vacuum and in the reaction field model for aqueous solvent. While the thermodynamic driving forces differ quantitatively in the different nanocage environments, qualitatively the product is amply favored in all cases. Again, the halogenated form of the RS has an enormous activation barrier regardless

of the Ga^{3+} vs Si^{3+} construct. But the most distinguishing characteristic is that while both tetrahedral assemblies lower the barrier to reductive elimination for the $P(CH_3)_3(CH_3)_2Au^+$ relative to the halogenated form, it is the Ga^{3+} nanocage that yields an activation barrier that is comparable to the free reactant state, while the barrier increases substantially for the Si^{4+} complex. The barrier increases in the reaction field for both supramolecular complexes, but the relative trends still hold, i.e. the greater acceleration of the alkyl-alkyl reductive elimination from $Ga_4L_6^{12-}$ compared to $Si_4L_6^{8-}$.

Overall the reaction field model misses important molecular effects of the solvated environment. Therefore we consider a more detailed molecular environment that includes internal water and counterions to provide greater clarification as to the differences between the two tetrahedral assemblies. In this case, the $Ga_4L_6^{12-}$ and $Si_4L_6^{8-}$ capsules are augmented with K^+ counterions (derived from the reported crystal structure[19]) and three resolved water molecules inside the capsule (see Methods). In Table 2 we provide the binding energy, E_{bind},

$$E_{bind} = E^{opt}_{complex-capsule} - E^{opt}_{complex} - E^{opt}_{capsule} \quad (1)$$

where the structure of the complex and capsule are reoptimized in vacuum prior to energy calculation to account for the reorganization costs.

Table 2 Binding (E_{bind}) energies in kcal/mol of $P(CH_3)_3(CH_3)_2AuI$ and $P(CH_3)_3(CH_3)_2Au^+$ in $Ga_4L_6^{12-}$ and $Si_4L_6^{8-}$ in both RS and PS. Here, the tetrahedral assembly is modeled with K^+ counterions and water molecules inside the cavity. See Table 1 for more detail.

Stationary Point	Active Complex	Metal Complex	E_{Bind} (vacuum)	E_{Bind} (reaction field)
Reactant State	$P(CH_3)_3(CH_3)_2AuI$	$Ga_4L_6^{12-}$	-12.7	-19.6
		$Si_4L_6^{8-}$	8.6	6.6
	$P(CH_3)_3(CH_3)_2Au^+$	$Ga_4L_6^{12-}$	-115.7	-121.9
		$Si_4L_6^{8-}$	-55.0	-89.6
Product State	$P(CH_3)_3(CH_3)_2AuI$	$Ga_4L_6^{12-}$	-7.8	11.0
		$Si_4L_6^{8-}$	18.4	13.0
	$P(CH_3)_3(CH_3)_2Au^+$	$Ga_4L_6^{12-}$	-57.7	-77.9
		$Si_4L_6^{8-}$	-30.5	-52.7

We see that both the Ga and Si capsules bind the $P(CH_3)_3(CH_3)_2Au^+$ preferably to $P(CH_3)_3(CH_3)_2AuI$ by ~60-100 kcal/mole, as would be expected from simple electrostatic arguments, and consistently explains the drive of the halide dissociation step towards the formation of $P(CH_3)_3(CH_3)_2Au^+$ as shown in Figure 1. This is also consistent with the work of Frushicheva

et al. that demonstrated that $Ga_4L_6^{12-}$ stabilizes positively charged species over uncharged molecules.[20] Furthermore, we observe that both capsules bind the RS species better than PS species, which is a signature of some efficiency in catalytic turnover, and which is best optimized for the $Ga_4L_6^{12-}$ cage. These exact same trends are robust if a continuum model for solvent is included.

Finally, we consider the effect of a more extended molecular solvate environment for the two capsules on the energy barrier of the reductive elimination from $P(CH_3)_3(CH_3)_2Au^+$, the preferably encapsulated reactive complex, that now includes a first solvation shell (Figure 3a). We find that the activation energy barrier is only ~5.5 kcal/mol when $P(CH_3)_3(CH_3)_2Au^+$ is encapsulated in $Ga_4L_6^{12-}$, compared with ~24.4 kcal/mol when encapsulated in $Si_4L_6^{8-}$ (Figure 3b). This is consistent with the experimental observation[21] that $Si_4L_6^{8-}$ catalyzes other reactions less efficiently than $Ga_4L_6^{12-}$, a result that appears general and extensible to the alkyl-alkyl reductive elimination from the Au(III) complex.

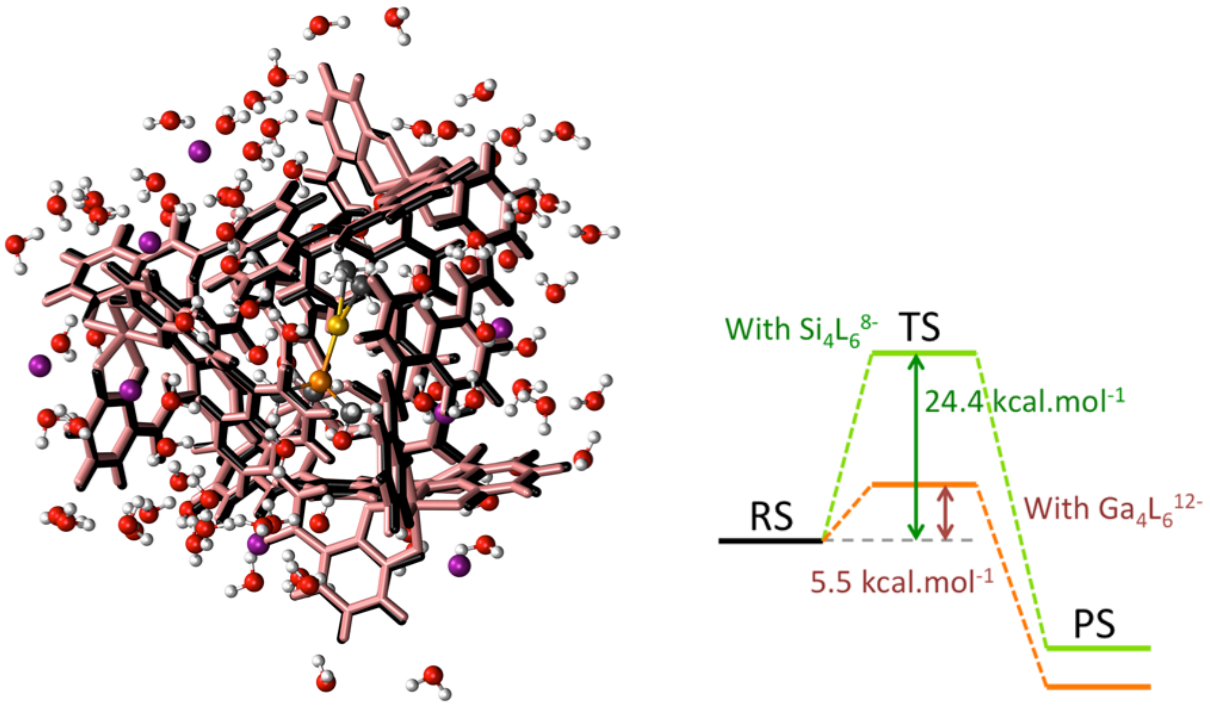

Figure 3. (a) Optimized geometry of $P(CH_3)_3(CH_3)_2Au^+$ encapsulated in $Ga_4L_6^{12-}$ with first solvation shell and counter-ions. The optimized $Si_4L_6^{8-}$ structure is superimposed in purple for comparison. (b) Energy barrier of the reductive elimination reaction from $P(CH_3)_3(CH_3)_2Au^+$ in $Ga_4L_6^{12-}$ and $Si_4L_6^{8-}$. The structure of the transition state (TS) of the whole system was determined by placing the TS structure of $P(CH_3)_3(CH_3)_2Au^+$ determined in vacuum and placing it in the capsule through minimization of the RMSD with the RS geometry in the capsule. The TS of the complex was then kept fixed while relaxing the capsule, water and ions around it.

To further check that the water molecules inside the cavity were not responsible for the energy barrier difference observed for the two capsules, we computed the energy of RS and TS in their absence. After removing the 3 interior water molecules, there remains a ~18 kcal/mol difference between $P(CH_3)_3(CH_3)_2Au^+$ encapsulated in $Ga_4L_6^{12-}$ and $Si_4L_6^{8-}$. Since the geometry of the two capsules are nearly identical, including the position and orientation of the water molecules inside the cavity after optimization, we conclude that the difference in the energy barrier primarily comes from electrostatic interactions introduced by the tetrahedral capsule. This does not mean that the water molecules inside the complex are not important, but rather that they have a similar energetic contribution for both $Ga_4L_6^{12-}$ and $Si_4L_6^{8-}$, leaving only electrostatic differences to explain the accelerated performance of the Ga over the Si assemblies for the reductive elimination reaction. This is confirmed when we embed the extended solvated capsules within a reaction field to account for long-ranged electrostatic effects, in which we find that the activation energy barrier increases to ~18.3 kcal/mol for the reactant encapsulated in $Ga_4L_6^{12-}$ but is still significantly smaller than E_A~25.8 kcal/mol for $Si_4L_6^{8-}$, translating to ~5 order of magnitude improvement in catalytic rate for the Ga complex. This is consistent with the results of Hong and co-workers who demonstrated that when the anionic host charge is reduced by using the self-assembled tetrahedral complex $Si_4L_6^{8-}$, the reaction rate for Nazarov cyclization decreases by 2-3 orders of magnitude.[21]

In summary, we presented high level DFT calculations of gold complexes in vacuum and encapsulated within a supramolecular tetrahedral assembly $Ga_4L_6^{12-}$ and $Si_4L_6^{8-}$, in which the latter assembly has been applied to carbon-carbon reductive elimination for the first time. We quantified the preference of both negatively charged capsules for binding the cation intermediate $P(CH_3)_3(CH_3)_2Au^+$ over the square planar complex $P(CH_3)_3(CH_3)_2AuI$. Further, we showed that the reductive elimination reaction has a lower energy barrier from $P(CH_3)_3(CH_3)_2Au^+$ than $P(CH_3)_3(CH_3)_2AuI$. Finally, by comparing the activation barrier for reductive elimination from the preferred $P(CH_3)_3(CH_3)_2Au^+$ reactant when encapsulated within the solvated $Ga_4L_6^{12-}$ and $Si_4L_6^{8-}$ capsules, we were able to identify electrostatic interactions as being the main factor of the transition state stabilization (given the large difference in charge) and thus differences in reaction rates seen for Ga vs. Si. Future work will perform condensed phase simulations for a full molecular solvent environment of the tetrahedral assemblies to build a conformational ensemble and better ascertain the role of electric fields and their role in the catalytic performance of these synthetic catalysts.[18]

ACKNOWLEDGEMENT. This work was supported by the Director, Office of Science, Office of Basic Energy Sciences, Chemical Sciences Division of the U.S. Department of Energy under Contract No. DE-10AC02-05CH11231. This research used resources of the National Energy Research Scientific Computing Center, a DOE Office of Science User Facility supported by the Office of Science of the U.S. Department of Energy under Contract No. DE-AC02-05CH11231.

METHODS. The geometries of the reactant (RS) and product (PS) states were optimized with Density Functional Theory (DFT) using the dispersion corrected meta-generalized gradient approximation (GGA) functional B97M-V[22-23] in combination with a DZVP basis set optimized for multigrid integration[24] as implemented in the CP2K software package[25-26]. All calculations presented here were performed with periodic boundary conditions (30Å×30Å×30Å), 5 grids and a cutoff of 400 Ry. The structure of the transition state (TS) were obtained with the dimer method in CP2K[25] and validated against the geometries computed with Q-Chem[27] using the B3LYP and M06 functionals. The TS structures are also characterized by a single imaginary frequency.

The starting geometry of the encapsulated complex system was built by positioning the vacuum optimized gold complex geometry in the capsule minimizing the root-mean-square-displacement (RMSD) with the X-ray structure of bis(trimethylphosphine) gold cation in $Ga_4L_6^{12-}$ (coordinates provided as Supplementary Data in [19]). Further, the system was solvated into a 30Å x 30Å x 30Å water box and all water molecules were then removed but the ones within the cavity. Potassium counter ions were also included at the positions provided in the X-ray resolved structure[19]. The resulting structures were then optimized with DFT as described above. The $Si_4L_6^{8-}$ assembly was build by replacing the Ga vertices by Si atoms prior to optimization. All calculations that report a self-consistent reaction field (SCRF) utilized the methodology outlined by Bashford and co-workers[28], and has been implemented in the CP2K program.

REFERENCES

1. Jia, H.-P.; Quadrelli, E. A. Mechanistic Aspects of Dinitrogen Cleavage and Hydrogenation to Produce Ammonia in Catalysis and Organometallic Chemistry: Relevance of Metal Hydride Bonds and Dihydrogen. *Chem. Soc. Rev.* **2014,** *43*, 547-564.
2. Nelson, D. J.; Nolan, S. P. Hydroxide Complexes of the Late Transition Metals: Organometallic Chemistry and Catalysis. *Coord. Chem. Rev.* **2017,** *353*, 278-294.
3. Bertrand, B.; Casini, A. A Golden Future in Medicinal Inorganic Chemistry: The Promise of Anticancer Gold Organometallic Compounds. *Dalton Trans.* **2014,** *43*, 4209-4219.
4. Cherney, A. H.; Kadunce, N. T.; Reisman, S. E. Enantioselective and Enantiospecific Transition-Metal-Catalyzed Cross-Coupling Reactions of Organometallic Reagents to Construct C-C Bonds. *Chem. Rev.* **2015,** *115* (17), 9587-9652.

5. Shin, K.; Kim, H.; Chang, S. Transition-Metal-Catalyzed C-N bond Forming Reactions Using Organic Azides as the Nitrogen Source: A Journey for the Mild and Versatile C-H Amination. *Acc. Chem. Res.* **2015,** *48* (4), 1040-1052.
6. Wang, Q.; Su, Y.; Li, L.; Huang, H. Transition-metal Catalysed C-N Bond Activation. *Chem. Soc. Rev.* **2016,** *45*, 1257-1272.
7. Arrechea, P. L.; Buchwald, S. L. Biaryl Phosphine Based Pd(II) Amido Complexes: The Effect of Ligand Structure On Reductive Elimination. *J. Am. Chem. Soc.* **2016,** *138* (38), 12486-12493.
8. Bour, J. R.; Camasso, N. M.; Meucci, E. A.; Kampf, J. W.; Canty, A. J.; Sanford, M. S. Carbon-Carbon bond-Forming Reductive Elimination From Isolated Nickel(III) Complexes. *J. Am. Chem. Soc.* **2016,** *138* (49), 16105-16111.
9. Hartwig, J. F. Electronic Effects on Reductive Elimination to Form Carbon-Carbon and Carbon-Heteroatom Bonds from Palladium(II) Complexes. *Inorg. Chem.* **2007,** *46* (6), 1936-1947.
10. Perez-Rodriguez, M.; Braga, A. A. C.; Garcia-Melchor, M.; Perez-Temprano, M. H.; Casares, J. A.; Ujaque, G.; de Lera, A. R.; Alvarez, R.; Maseras, F.; Espinet, P. C-C Reductive Elimination in Palladium Complexes, and the Role of Coupling Additives. A DFT Study Supported by Experiment. *J. Am. Chem. Soc.* **2009,** *131* (10), 3650-3657.
11. Perez-Temprano, M. H.; Racowski, J. M.; Kampf, J. W.; Sanford, M. S. Competition Between Sp3-C-N Vs Sp3-C-F Reductive Elimination from Pd(IV) Complexes. *J. Am. Chem. Soc.* **2014,** *136* (11), 4097-4100.
12. Pendleton, I. M.; Perez-Temprano, M. H.; Sanford, M. S.; Zimmerman, P. M. Experimental and Computational Assessment of Reactivity and Mechanism in C(Sp3)-N Bond-Forming Reductive Elimination From Palladium(IV). *J. Am. Chem. Soc.* **2016,** *138* (18), 6049-6060.
13. Wolf, W. J.; Winston, M. S.; Toste, F. D. Exceptionally Fast Carbon--Carbon Bond Reductive Elimination from Gold(III). *Nat. Chem.* **2013,** *6*, 159-164.
14. Nijamudheen, A.; Karmakar, S.; Datta, A. Understanding the Mechanisms of Unusually Fast HH, CH, and CC Bond Reductive Eliminations from Gold(III) Complexes. *Chem. Eur. J.* **2014,** *20* (45), 14650-14658.
15. Komiya, S.; Kochi, J. K. Electrophilic Cleavage of Organogold Complexes with Acids. The Mechanism of the Reductive Elimination of Dialkyl(Aniono)Gold(III) Species. *J. Am. Chem. Soc.* **1976,** *98* (24), 7599-7607.
16. Kaphan, D. M.; Levin, M. D.; Bergman, R. G.; Raymond, K. N.; Toste, F. D. A Supramolecular Microenvironment Strategy for Transition Metal Catalysis. *Science* **2015,** *350* (6265), 1235-1238.
17. Caulder, D. L.; Raymond, K. N. Supermolecules by Design. *Acc. Chem. Res.* **1999,** *32* (11), 975-982.
18. Welborn, V. V.; Pestana, L. R.; Head-Gordon, T. Perspective: Computational Optimization of Electric Fields for Better Catalysis Design. *Nature Catal.* **2018,** *accepted*.
19. Levin, M. D.; Kaphan, D. M.; Hong, C. M.; Bergman, R. G.; Raymond, K. N.; Toste, F. D. Scope and Mechanism of Cooperativity at the Intersection of Organometallic and Supramolecular Catalysis. *J. Am. Chem. Soc.* **2016,** *138* (30), 9682-9693.
20. Frushicheva, M. P.; Mukherjee, S.; Warshel, A. Electrostatic Origin of the Catalytic Effect of a Supramolecular Host Catalyst. *J. Phys. Chem. B* **2012,** *116* (45), 13353-13360.
21. Hong, C. M.; Morimoto, M.; Kapustin, E. A.; Alzakhem, N.; Bergman, R. G.; Raymond, K. N.; Toste, F. D. Deconvoluting the Role of Charge in a Supramolecular Catalyst. *J. Am. Chem. Soc.* **2018,** *in press*.

22. Mardirossian, N.; Head-Gordon, M. Mapping the Genome of Meta-Generalized Gradient Approximation Density Functionals: The Search for B97M-V. *J. Chem. Phys.* **2015,** *142* (7), 074111.
23. Mardirossian, N.; Head-Gordon, M. Thirty Years of Density Functional Theory in Computational Chemistry: An Overview and Extensive Assessment of 200 Density Functionals. *Mol. Phys.* **2017,** *115* (19), 2315-2372.
24. VandeVondele, J.; Hutter, J. Gaussian Basis Sets for Accurate Calculations on Molecular Systems in Gas and Condensed Phases. *J. Chem. Phys.* **2007,** *127* (11), 114105-114105.
25. Hutter, J.; Iannuzzi, M.; Schiffmann, F.; VandeVondele, J. CP2K: Atomistic Simulations of Condensed Matter Systems. *Wiley Interdisc. Rev.: Comput. Mol. Sci.* **2013,** *4* (1), 15-25.
26. VandeVondele, J.; Krack, M.; Mohamed, F.; Parrinello, M.; Chassaing, T.; Hutter, J. Quickstep: Fast and Accurate Density Functional Calculations Using a Mixed Gaussian and Plane Waves Approach. *Comput. Phys. Commun.* **2005,** *167* (2), 103-128.
27. Shao, Y.; Gan, Z.; Epifanovsky, E.; Gilbert, A. T. B.; Wormit, M.; Kussmann, J.; Lange, A. W.; Behn, A.; Deng, J.; Feng, X. *et al.* Advances in Molecular Quantum Chemistry Contained in the Q-Chem 4 Program Package. *Mol. Phys.* **2015,** *113* (2), 184-215.
28. Chen, J. L.; Noodleman, L.; Case, D. A.; Bashford, D. Incorporating Solvation Effects Into Density Functional Electronic Structure Calculations. *J. Phys. Chem.* **1994,** *98*, 11059-11068.